Femtosecond-laser generation of self-organized bubble patterns in fused silica

Yves Bellouard[1,*] and Max-Olivier Hongler[2]

[1]*Mechanical Engineering Dept, Eindhoven University of Technology, Eindhoven, The Netherlands*
[2]*School of Engineering, Ecole Polytechnique Fédérale de Lausanne, Lausanne, Switzerland*
**y.bellouard@tue.nl*

Abstract: By continuously scanning a femtosecond laser beam across a fused silica specimen, we demonstrate the formation of self-organized bubbles buried in the material. Rather than using high intensity pulses and high numerical aperture to induce explosions in the material, here bubbles form as a consequence of cumulative energy deposits. We observe a transition between chaotic and self-organized patterns at high scanning rate (above 10 mm/s). Through modeling the energy exchange, we outline the similarities of this phenomenon with other non-linear dynamical systems. Furthermore, we demonstrate with this method the high-speed writing of two- and three- dimensional bubble "crystals" in bulk silica.

©2011 Optical Society of America

OCIS codes: (140.7090) Ultrafast lasers; (160.2750) Glass and other amorphous materials; (320.2250) Femtosecond phenomena; (320.7130) Ultrafast processes in condensed matter, including semiconductors.

References and links

1. K. M. Davis, K. Miura, N. Sugimoto, and K. Hirao, "Writing waveguides in glass with a femtosecond laser," Opt. Lett. **21**(21), 1729–1731 (1996).
2. S. Nolte, M. Will, J. Burghoff, and A. Tuennermann, "Femtosecond waveguide writing: a new avenue to three-dimensional integrated optics," Appl. Phys., A Mater. Sci. Process. **77**(1), 109–111 (2003).
3. G. Della Valle, S. Taccheo, R. Osellame, A. Festa, G. Cerullo, and P. Laporta, "1.5 mum single longitudinal mode waveguide laser fabricated by femtosecond laser writing," Opt. Express **15**(6), 3190–3194 (2007), http://www.opticsinfobase.org/oe/abstract.cfm?URI=oe-15-6-3190.
4. Y. Shimotsuma, P. G. Kazansky, J. Qiu, and K. Hirao, "Self-organized nanogratings in glass irradiated by ultrashort light pulses," Phys. Rev. Lett. **91**(24), 247405 (2003).
5. Q. Sun, F. Liang, R. Vallée, and S. L. Chin, "Nanograting formation on the surface of silica glass by scanning focused femtosecond laser pulses," Opt. Lett. **33**(22), 2713–2715 (2008).
6. E. N. Glezer and E. Mazur, "Ultrafast-laser driven micro-explosions in transparent materials," Appl. Phys. Lett. **71**(7), 882–884 (1997).
7. S. Juodkazis, K. Nishimura, S. Tanaka, H. Misawa, E. G. Gamaly, B. Luther-Davies, L. Hallo, P. Nicolai, and V. T. Tikhonchuk, "Laser-induced microexplosion confined in the bulk of a sapphire crystal: evidence of multimegabar pressures," Phys. Rev. Lett. **96**(16), 166101 (2006).
8. S. Rajesh and Y. Bellouard, "Towards fast femtosecond laser micromachining of fused silica: The effect of deposited energy," Opt. Express **18**(20), 21490–21497 (2010), http://www.opticsinfobase.org/oe/abstract.cfm?URI=oe-18-20-21490.
9. C. Schaffer, J. García, and E. Mazur, "Bulk heating of transparent materials using a high-repetition-rate femtosecond laser," Appl. Phys., A Mater. Sci. Process. **76**(3), 351–354 (2003).
10. S. Eaton, H. Zhang, P. Herman, F. Yoshino, L. Shah, J. Bovatsek, and A. Arai, "Heat accumulation effects in femtosecond laser-written waveguides with variable repetition rate," Opt. Express **13**(12), 4708–4716 (2005), http://www.opticsinfobase.org/oe/abstract.cfm?URI=oe-13-12-4708.
11. R. Graf, A. Fernandez, M. Dubov, H. Brueckner, B. Chichkov, and A. Apolonski, "Pearl-chain waveguides written at megahertz repetition rate," Appl. Phys. B **87**(1), 21–27 (2007).
12. E. Toratani, M. Kamata, and M. Obara, "Self-fabrication of void array in fused silica by femtosecond laser processing," Appl. Phys. Lett. **87**(17), 171103 (2005).
13. T. Hashimoto, S. Juodkazis, and H. Misawa, "Void formation in glasses," N. J. Phys. **9**(8), 253 (2007).
14. J. Song, X. Wang, X. Hu, Y. Dai, J. Qiu, Y. Cheng, and Z. Xu, "Formation mechanism of self-organized voids in dielectrics induced by tightly focused femtosecond laser pulses," Appl. Phys. Lett. **92**(9), 092904 (2008).
15. X. Wang, F. Chen, Q. Yang, H. Liu, H. Bian, J. Si, and X. Hou, "Fabrication of quasi-periodic micro-voids in fused silica by single femtosecond laser pulse," Appl. Phys., A Mater. Sci. Process. **102**(1), 39–44 (2011).

#142538 - $15.00 USD Received 10 Feb 2011; revised 6 Mar 2011; accepted 9 Mar 2011; published 24 Mar 2011
(C) 2011 OSA

16. S. Juodkazis, H. Misawa, and I. Maksimov, "Thermal accumulation effect in three-dimensional recording by picosecond pulses," Appl. Phys. Lett. **85**(22), 5239–5241 (2004).
17. W. Yang, P. G. Kazansky, Y. Shimotsuma, M. Sakakura, K. Miura, and K. Hirao, "Ultrashort-pulse laser calligraphy," Appl. Phys. Lett. **93**(17), 171109 (2008).
18. W. Yang, P. G. Kazansky, and Y. P. Svirko, "Non-reciprocal ultrafast laser writing," Nat. Photonics **2**(2), 99–104 (2008).
19. B. Poumellec, M. Lancry, J. C. Poulin, and S. Ani-Joseph, "Non reciprocal writing and chirality in femtosecond laser irradiated silica," Opt. Express **16**(22), 18354–18361 (2008), http://www.opticsinfobase.org/oe/abstract.cfm?URI=oe-16-22-18354.
20. D. N. Vitek, E. Block, Y. Bellouard, D. E. Adams, S. Backus, D. Kleinfeld, C. G. Durfee, and J. A. Squier, "Spatio-temporally focused femtosecond laser pulses for nonreciprocal writing in optically transparent materials," Opt. Express **18**(24), 24673–24678 (2010), http://www.opticsinfobase.org/oe/abstract.cfm?URI=oe-18-24-24673.
21. C. E. Brennen, *Cavitation and Bubble Dynamics* (Oxford University Press, 1995).
22. X. Xu and D. A. Willis, "Non-equilibrium phase change in metal induced by nanosecond pulsed laser irradiation," J. Heat Transfer **124**(2), 293–298 (2002).
23. J. Guckenheimer and P. Holmes, *Nonlinear Oscillations, Dynamical Systems and Bifurcations of Vector Fields*, Vol. 42 of Applied Mathematical Sciences (Springer, 1983), Section 2.4.
24. V. I. Goryunov, A. V. Dondoshanskaya, V. S. Metrikin, and R. F. Nagaev, "Periodic motions of an object above a surface vibrating according to an anharmonic law," Prikl. Mekh. **10**, 65–71 (1974).
25. M. C. Ruzicka, "Dripping faucet and bubbling faucet: an analogy," Chem. Eng. Res. Des. **87**(10), 1366–1370 (2009).

1. Introduction

Femtosecond pulses focused in a glass substrate induce various modifications in the material depending on the fluence level. Upon increasing pulse energies above the energy threshold for non-linear absorption, femtosecond laser exposure leads to an increase of the refractive index [1–3], the formation of nano-gratings [4,5], or to micro-explosions [6,7]. The intensity of the modifications also depends on the amount of energy deposited in the material [8]. Cumulative effects may be observed for repetition rates above 1 MHz [9,10]. In this regime, the limited temporal separation between pulses becomes relevant and marks the onset for bulk heating dynamics.

In this paper, we focus on this cumulative regime (repetition rate >1 MHz) and study the role of the scanning speed on the structures formed in the material when exposed to low-energy pulses. In particular, we show that for high-speed scanning rates, self-organized bubble networks are created. While the formation of voids in silica glass has been studied in the past by several authors following the seminal work from Glezer *et al.* [6], those were obtained with high NA focusing optics and high focused intensity of single pulses (see for instance [6,12–15]). Using a different mechanism, R. Graf *et al*. [11] demonstrated the formation of 'pearl-chain' structures by continuously scanning short pulses (sub-30fs, <40 nJ, NA = 0.55) emitted at high-repetition rates from an oscillator (10 MHz). These pearl-chain structures consist of periodically distributed bubbles. Interestingly, the authors demonstrated that these structures have waveguiding properties. Using a similar principle, here we explore - both experimentally and theoretically - the dynamics of complex bubble patterns formation in the cumulative regime (9.8 MHz) using low NA and low energy pulses. In particular, we analyze the conditions for bubble formation and identify transitions from chaotic to periodic regimes. Finally, we demonstrate how this process can be used to create two- and three- dimensional bubble 'crystals', opening interesting fundamental and industrial perspectives.

2. Experiments

2.1. Methods: Laser setup, specimens used and observations methods used

We use a diode-pumped Ytterbium-KGW based femtosecond oscillator (Amplitude Systèmes, t-Pulse 500, optimized for short pulse generation) delivering 380fs pulses at 1024 nm. The oscillator emits pulses at a frequency of 9.4 MHz. For these experiments, we focus pulses with energy ranging from 180nJ to a maximum of 450 nJ. To focus the beam, we use a commercial microscope objective with a numerical aperture of 0.3. The specimens used are

#142538 - $15.00 USD Received 10 Feb 2011; revised 6 Mar 2011; accepted 9 Mar 2011; published 24 Mar 2011
(C) 2011 OSA

cuboids of OH-rich fused silica (Dynasil and Suprasil, OH = 1000 ppm) that are moved under the laser beam using commercial positioning stages (Physik Instrument). Patterns are written by moving the sample under the laser beam in a direction perpendicularly to the laser optical propagation axis, at velocities varying from 0.5 mm/s to 32 mm/s (the maximum speed of our stages). The pulse energies are measured at the focal point. Images of the laser-treated samples are taken with an optical microscope (20X and 50X magnifications) equipped with a Nomarski Interference Contrast enhancement and cross-polarizers. For the observation of the three-dimensional patterns, we use dark field imaging to reveal bubble layers buried deep in the material.

2.2. Effect of writing speed and direction

In a first experiment, line patterns three centimeter long were written across the specimen at a depth of about 190 +/– 10 μm below the surface. The top-view and side-view microscope images of these lines patterns are shown in Figs. 1 and 2, respectively.

The speed was gradually increased from 5 to 30 mm/s while the pulse energy was maintained constant. Lines were written in both directions (the writing direction is indicated by an arrow on the figure). The lateral separations between lines vary from 100 to 300 μm.

We observe two characteristic regimes. At low speeds, erratic patterns characterized by randomly sized bubbles separated by random space intervals are formed. This regime is chaotic. As the speed increases (typically above 10 mm/s), self-organized patterns appear with varying complexity and periodicity. These patterns are characterized by an outer shell of modified material inside which well-defined cavities are found (with a dark appearance due to total internal reflection associated with bottom-light illumination). The complexity of these patterns gradually decreases and ultimately converges to its simplest form, a single spherical cavity (found at and above 30 mm/s in Fig. 1). Most remarkable is the regularity of these patterns: the periodicity accuracy is better than a micron. This suggests a very stable formation mechanism, immune from noise generally present in such complex dynamic system. Interestingly, we observe a strong dependence of these patterns with the writing direction. Anisotropic writing in isotropic material first reported by Kazansky *et al.* [17], has been since observed by several authors [18–20] in the non-cumulative regime. Here we observe it in the cumulative regime as can be seen in Fig. 1. This anisotropy could be due to a pulse front tilt as suggested in [17] or to an imperfect symmetry of the laser spot energy distribution.

Figure 2 shows the structures of the Fig. 1 patterns from the plane orthogonal to the writing direction. Together with the optical microscope images shown on the left side, a scanning electron microscope (SEM) image of a different specimen (but produced with similar exposing conditions) is shown on the right. This specimen was grinded over several tens of microns in its thickness, polished and etched for 15 min in a low-concentration HF bath (according the procedure described in [8]) in order to observe an exposed-region representative of the features present in the bulk.

The laser-affected-zones (LAZ) consist of elongated comet-like shapes. The envelopes (or outer shell) of these structures are rather large: The shells dimensions depend on the numerical aperture. For a NA of 0.3, these structures are about 30 μm in diameter and 75 μm in length. At higher NA, i.e. tighter focusing conditions, for the same pulse energy parameters, the size of the bubble and its surrounding shell are significantly smaller. In Fig. 2 (left), the size of the largest bubbles are about 10 μm and are therefore much bigger than the laser spot (about 2μm for the NA = 0.3 objective). The tails of these 'comets' seem to contain cracks, possibly originating from a high stress concentration induced by a high thermal gradient. The presence of cracks at the tail is confirmed by the SEM observation shown in Fig. 2 (right). The SEM image also indicates that these laser affected regions etched at a higher speed than the bulk.

#142538 - $15.00 USD Received 10 Feb 2011; revised 6 Mar 2011; accepted 9 Mar 2011; published 24 Mar 2011
(C) 2011 OSA

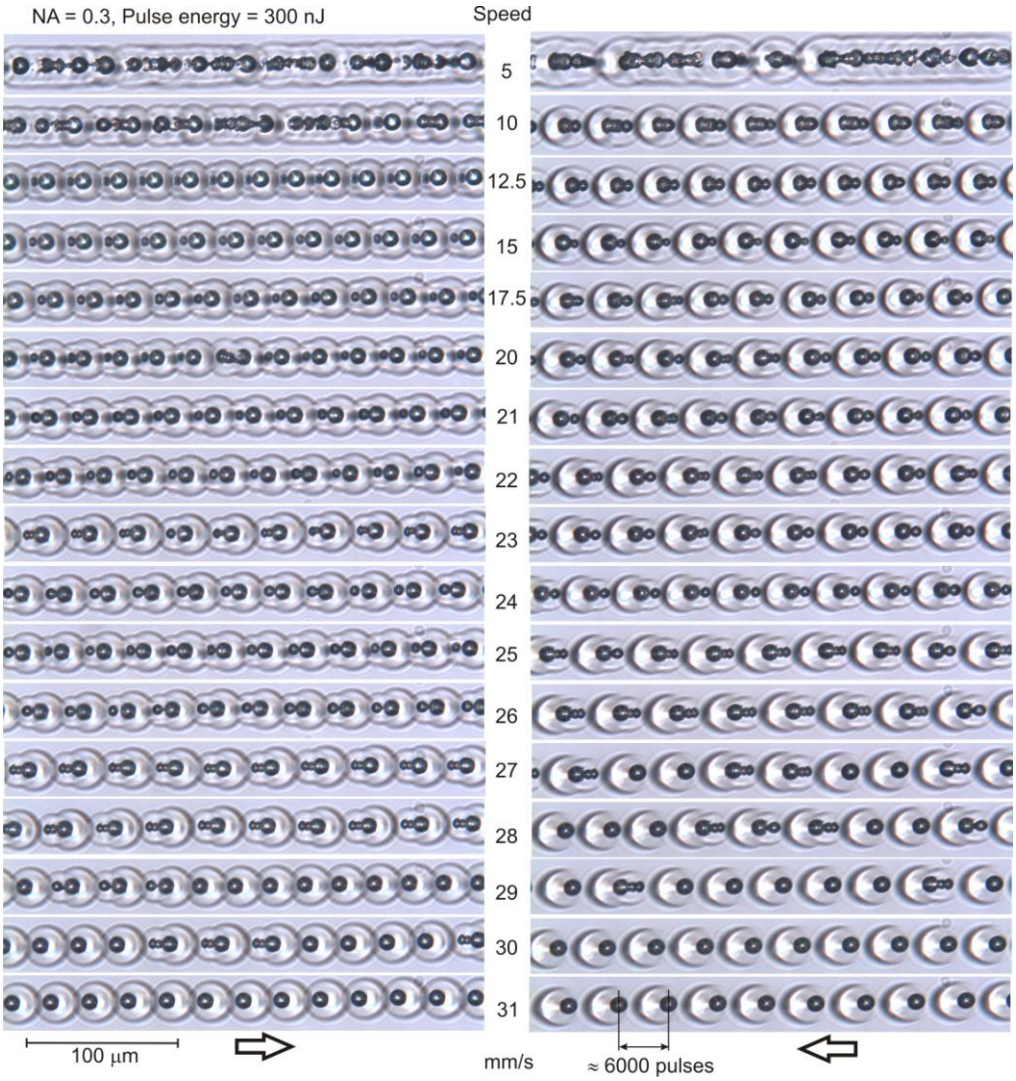

Fig. 1. Effect of increasing writing speeds: top-view microscopic images (bright field, bottom illumination). All the lines are written with the same pulse energy (300 nJ). The repetition rate is 9.4 MHz. The images on the right are lines written in the opposite direction from the ones shown on the left side and for the same velocity parameters. (The writing direction is indicated by an arrow at the bottom of the figure.) Lines are located 190 +/– 10μm below the surface. The images are taken with a bottom illumination.

Analyzing the data from Fig. 1 and Fig. 2, we see that the smallest bubbles are found at greater depths and were formed before the larger ones. At higher speeds, i.e. when the patterns are highly periodic, the lines behave as waveguides (this is visible in Fig. 2 where some of the light from the optical microscope light source is guided by - and only by - the periodic structure written at the highest speed). Note that this guiding mechanism is consistent with observations reported in [11]. The fact that only the most periodic structures guide light, points toward a grating-coupling waveguiding mechanism. The work reported in [16] suggests that similar regular bubble patterns may also be found in the picoseconds exposure regime.

#142538 - $15.00 USD Received 10 Feb 2011; revised 6 Mar 2011; accepted 9 Mar 2011; published 24 Mar 2011
(C) 2011 OSA

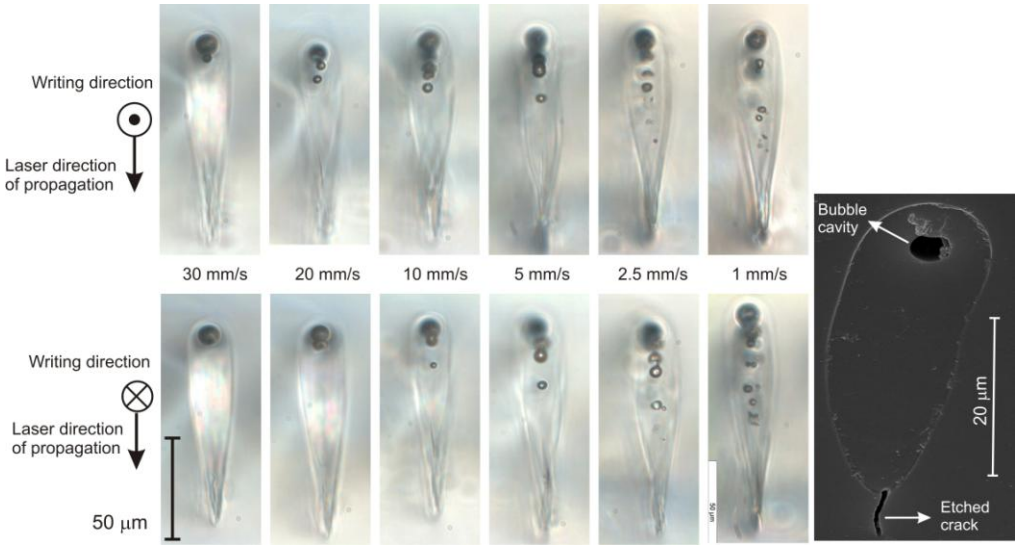

Fig. 2. Left: Effect of writing speeds, side view of bubble patterns. The patterns were written at increasing higher speeds. The pulse energy was 250 nJ. The NA was 0.3. Right: Typical 'single bubble pattern' as observed in a SEM. The specimen is viewed at an angle in the SEM and therefore, looks smaller than it is in reality. Pulse energy was 210 nJ. The laser affected zone has a comet shape in which bubbles are found.

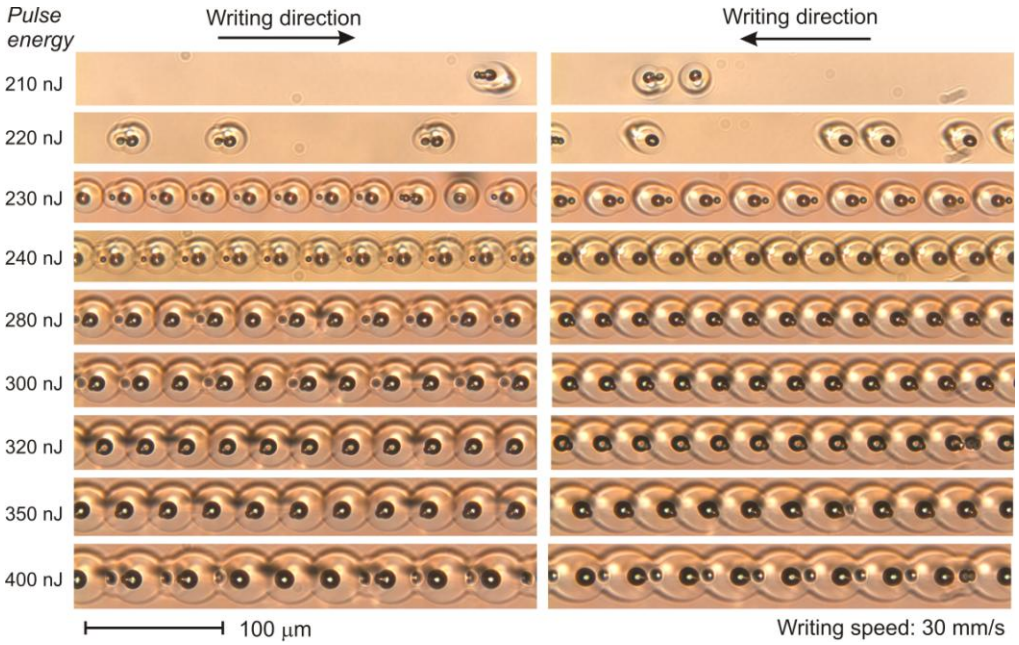

Fig. 3. Effect of increasing the pulse energy at a constant writing speed (30 mm/s). The patterns were written approximately 200 µm below the surface. The thermally affected zones surrounding bubbles are clearly visible (in particular at low energies where they are isolated one from another). The gradual increase of the laser affected zone width with the pulse energy is a clear signature of a thermal process.

Figure 3 illustrates lines patterns written at a constant speed but for increasing higher pulse energies (200 nJ to 400 nJ). Patterns were only visible for pulse energy above 210 nJ. For pulse energies below 220 nJ, the patterns are discontinuous and randomly spaced. Note that:

#142538 - $15.00 USD Received 10 Feb 2011; revised 6 Mar 2011; accepted 9 Mar 2011; published 24 Mar 2011
(C) 2011 OSA

- Although the experiments were performed above the threshold for non-linear absorption, we did not observe the formation of waveguides, or similar continuous patterns that would indicate a possible increase of the refractive index. The material present between the patterns seems Unot to be affected by the laser exposure. This effect could be due to the relatively low NA (0.3) used in these experiments.
- The shells defining the laser-affected zones were not observed independently of the presence of bubbles.
- Since groups consisting of several bubbles can be found isolated from other groups (as can be seen in Fig. 1 or at higher energy in Fig. 3), the formation of multiple bubbles in a single group does not seem to be a consequence of adjacent group interactions.

As the pulse energy is increased, the outer shell of the LAZ gets wider which is consistent with a temperature driven process. The bubbles, found within the LAZ, also grow in size with the pulse energy. In these experiments, from 280 nJ on, the largest bubbles are deformed along a diagonal, possibly as a result of an inhomogeneous energy distribution in the laser spot. Mirror symmetry between deformed large bubbles found in patterns written in opposite directions is also visible. From about 240 nJ on, the thermally affected zones overlap, possibly leading to additional interaction between groups containing bubbles.

2.3. Writing of two- and three- dimensional bubble networks: toward bubble crystals

Using the mechanism described in the previous section, lines of bubbles can be arranged spatially to form two- and three-dimensional patterns. Figure 4 shows a two-dimensional array formed by scanning multiple lines one after another at speed of 30 mm/s. All the lines were written along the same direction and were spaced regularly. In this example, one can see that the spatial frequency (indicated on the left) oscillates between two values. Figure 4 clearly exhibits the existence of an oscillation between two stable regimes (A and B).

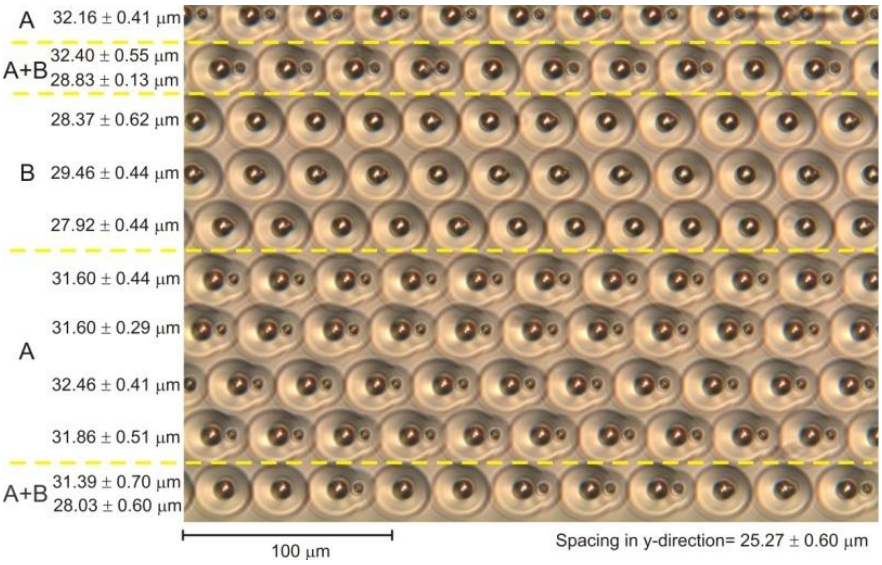

Fig. 4. Two-dimensional array of bubbles. Each line is written at 30mm/s and along the same direction.

#142538 - $15.00 USD Received 10 Feb 2011; revised 6 Mar 2011; accepted 9 Mar 2011; published 24 Mar 2011
(C) 2011 OSA

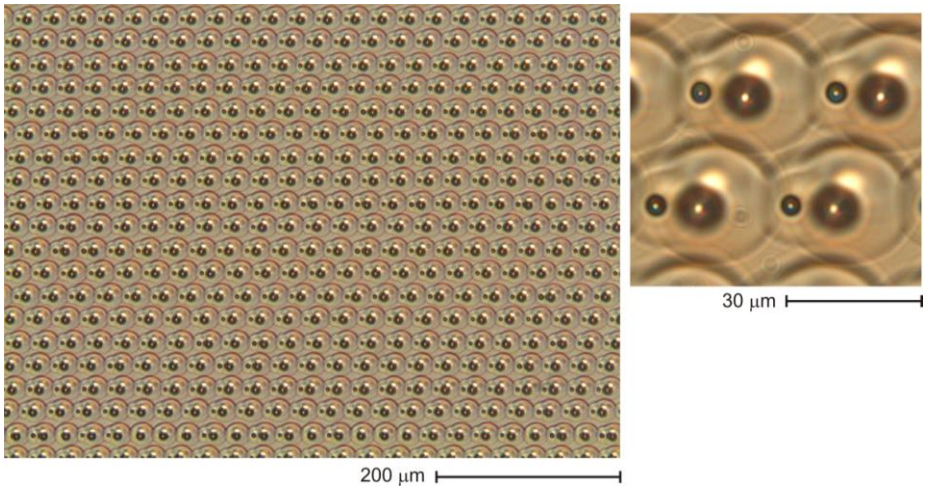

Fig. 5. Transmission optical microscope images of a large array of bubbles. The total area covered is 25 mm^2 and was written in less than a minute. The writing speed was 30 mm/s. The pattern here consists of a large bubble and a smaller one. The spacing between bubbles patterns is 31 μm. The inset shows a few bubbles seen at higher magnification. The image is focused on the smaller bubble illustrating the fact that large and small bubbles lie on different planes (a few μm apart).

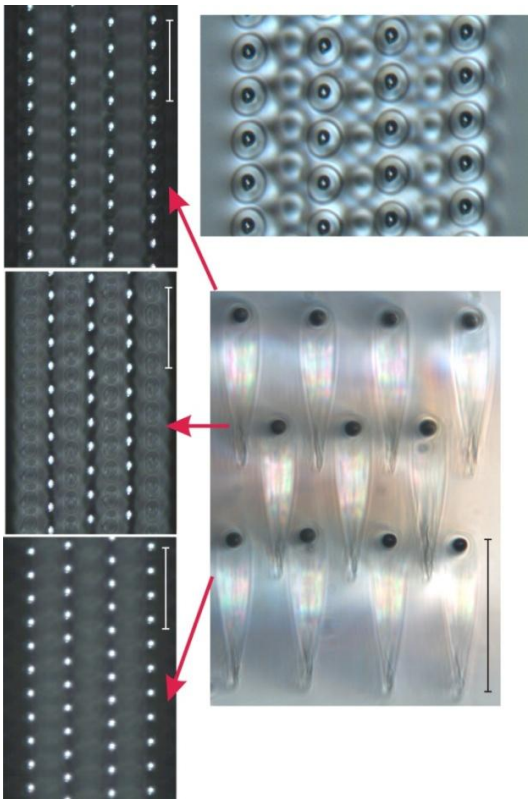

Fig. 6. Three-dimensional network of bubbles. Images are taken with an optical microscope (20X objective). The three images on the left are taken using dark-field microscopy and illustrate the regularity of the spatial arrangement. The bottom-right image shows the cross section of the 3D assembly and the top-right image a portion of the structure seen from the top surface. Scale bar is 100 μm.

#142538 - $15.00 USD Received 10 Feb 2011; revised 6 Mar 2011; accepted 9 Mar 2011; published 24 Mar 2011
(C) 2011 OSA

Figure 5 shows a very large array of bubbles written at constant speed (30 mm/s) and constant spacing between lines. This pattern covers a large area of the specimen (25 mm^2) and was written in less than a minute. It demonstrates the stunning stability of the patterns and underlines how such process can be used to efficiently write a bubble network. This writing method can be extended to the third dimension to form three-dimensional bubble crystals. As a demonstration, Fig. 6 shows a three dimensional pattern consisting of a set of lines written in three different planes. The dark field microscopic images on the left side illustrate the perfect periodicity of the patterns and the bright field microscopic images (right side of Fig. 6) show the spatial organization in the top and transverse plane.

3. Interpretation and modeling

3.1. Phenomenological interpretation

Although voids can be byproducts of a tightly focused, intense femtosecond laser pulse [6,13], the low energies used here preclude the formation of a void or a bubble from a single pulse trigger. Here, as evidenced in Fig. 1, several thousands of pulses (for instance, more than 6000 pulses at 30 mm/s) impact the material between two consecutives bubbles. The process is therefore intrinsically cumulative and of thermal origin. The mechanism of absorption remains non-linear since the bubbles form in the bulk where the laser is focused. Furthermore, the pulse energies involved in this experiment are just above the typical threshold for non-linear absorption.

To further explain the peculiarities of these thermally-induced micro-structures, we propose the following scenario. As a signature of a cumulative process, the time period between two pulses is smaller than the material heat relaxation constant. As successive pulses are focused into the specimen, the temperature gradually increases until it reaches the temperature at which bubble nucleation becomes possible. We assume that homogeneous bubble nucleation theory [21] is applicable here. We call E_b the bubble nucleation threshold. The rate of spontaneous bubble nucleation from a superheated state is:

$$J = \eta \exp\left(\frac{-E_b}{k_B T}\right) \quad with \quad \eta = N\sqrt{\left(\frac{3\sigma}{\pi m}\right)}$$

where N is the number density of the liquid (molecules/m^3), σ is the surface tension and *m* is the mass of a molecule. In liquids, simulation shows that the nucleation rate remains small for temperatures below 0.9Tc (where Tc is the critical temperature). An illustration reported in [22] gives a frequency of spontaneous nucleation to be approximately 0.1 s^{-1} cm^{-3} for temperatures near 0.89Tc; the frequency increases dramatically to 10^{21} s^{-1} cm^{-3} for temperatures near 0.91Tc.

In our case, due to rapid heating of the glass, a large amount of superheating is found and hence one would expect the nucleation rate to be definitely higher at lower scanning speed. This is in agreement with the observations of Fig. 2: far more bubbles are found at lower speeds, which is consistent with a higher nucleation rate.

Although the images shown in Figs. 1 and 2 can be seen as a snapshot of this dynamic process, we can draw useful observations regarding the sequence of events underlying the 'frozen-in-glass' bubbles network. Firstly, we note that smaller bubbles are formed before large ones and deeper in the glass. As the temperature and the size of the heat-affected zone gradually increase, the focal point shifts up toward the incoming laser beam and so do the bubble nucleation sites. Such a shifting-up motion of the bubble could be reinforced by Marangoni flows which tend to push bubbles toward the hottest point in the liquid. We interpret the formation of the larger bubbles mainly by the coalescence of smaller ones that keep on nucleating at an ever increasing rate as the temperature approaches a maximum. (Evidence of bubble coalescence events are qualitatively confirmed by Fig. 7 for instance.)

#142538 - $15.00 USD Received 10 Feb 2011; revised 6 Mar 2011; accepted 9 Mar 2011; published 24 Mar 2011
(C) 2011 OSA

The formation of the first 'seed bubbles' inherently modify the local heat transfer conditions and may substantially increase the material heating rate. This observation coupled with the random nature of the bubble nucleation process could explain why discontinuous patterns may form at very low-pulse energy close to the threshold for bubble formation (see Fig. 3, pulse energies of 210 nJ and 220 nJ).

The bubble growth rate as a result of ever-increasing coalescence events may exceed the scanning speed up to a point at which the laser beam propagation is altered, stopping the underlying non-linear absorption process. This would cause a cooling down below the bubble nucleation threshold. Once the laser beam has moved away from the bubble zone, the non-linear absorption restarts and the process starts again leading to the formation of the periodic structure.

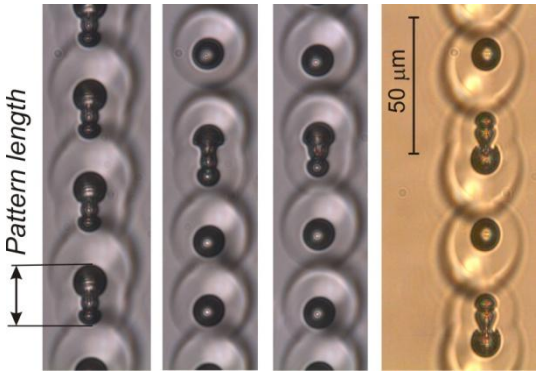

Fig. 7. Evidences of 'frozen-in' bubble coalescence events. These patterns were written with the conditions described in Fig. 1 (speed were 27 mm/s to 29 mm/s). The pattern length is shown. This parameter will be used in Fig. 11.

The formation of the chaotic bubble structures at lower speeds may be a consequence of several mechanisms. The spatial extension of the thermally affected zone (much larger at lower speeds) surrounding the laser spot allows for random nucleation in a wider area (within the LAZ), which ultimately yield random bubbles structures. In parallel, nonlinear energy dissipation mechanisms intimately connected with bubbles nucleation may trigger pseudo-deterministic behaviors giving rise to random bubble patterns.

Our present interpretation remains somehow speculative since we do not have yet a complete experimental set of observations enabling to build a refined microscopic picture of the physics of all phenomena underlying the generation of these patterns. However, the robustness and highly reproductive phenomena strongly suggests that the main features could be captured by a stylized model involving only a few variables. This interpretation is supported by a model (see below) that shows that such a system can evolve from a chaotic to a periodic regime.

3.2. Modeling

Let us consider a periodically flashing laser source S with pulse frequency f impacting on a piece of fused silica. For each laser pulse, we assume the energy to be uniformly distributed inside a disk of diameter w_0 (the beam waist). When the position of S is fixed in time, the energy accumulated inside the bulk can be idealized as:

$$\mathcal{E}(t) = \sum_k a_k \delta(t - k\Delta)$$

with $\Delta = 2\pi/f$ being the laser flashing period and a_k standing for the total absorbed energy contained in the single pulse k. The source S is moving with a uniform translation velocity v and our experimental conditions ensure that $v\Delta < w_0$.

#142538 - $15.00 USD Received 10 Feb 2011; revised 6 Mar 2011; accepted 9 Mar 2011; published 24 Mar 2011
(C) 2011 OSA

Accordingly, at a given location x, the accumulated energy $E_x(t)$ delivered to the material can be estimated as:

$$\mathcal{E}_x(t) \simeq \sum_{k=K_{\min}}^{K_{\max}} a_k \delta(t - k\Delta) \tag{1}$$

with

$$K_{\min} = \left[\frac{(x - w_0)}{vt} \right] \quad and \quad K_{\max} = \left[\frac{(x + w_0)}{vt} \right]$$

A sketch of the experimental situation is given in Fig. 8.

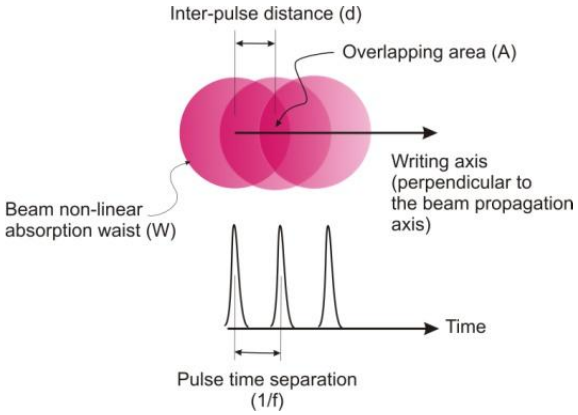

Fig. 8. Illustration of the deposition of energy in the system.

While the laser energy range precludes a single laser pulse from triggering a bubble nucleation, the local energy accumulation due to several successive pulses, as given by Eq. (1), produces bubbles inside the bulk as observed in Fig. 1. Although the phenomenon involves complex thermodynamics effects (bubble nucleation and coalescence, hydrodynamics effects, etc), we assume here that the pattern generation can effectively be described by a nucleation process. In this model, we call the nucleation threshold W_{cr}. In this view, the occurrence of a bubble pattern produces a sudden energy release.

As bubbles alter the specimen homogeneity, the laser energy absorption is locally modified. The v-translation of S implies that the laser spot will soon leave the bubble region thus enabling the original energy accumulation and surge scenario to be renewed. This alternation between accumulation and energy release renewals produces the velocity-dependent bubble patterns observed inside the bulk.

For a fixed energy of the laser pulses, the observed striking features reproduced in Fig. 1 can be summarized as follows:

a) generation of a strictly continuous energy accumulation of laser pulses rise to self-organized and fully reproducible bubble patterns,

b) occurrence of periodic patterns are highly regular despite the unavoidable presence of several potential noise sources,

c) by decreasing the translation velocity v, or consequently increasing the local energy, the patterns structures are modified leading to different periodicities, bubble sizes and ultimately for higher energy, to erratic patterns.

Our goal in this section is to propose a highly stylized model able to qualitatively reproduce the observed scenario of such patterns generation.

#142538 - $15.00 USD Received 10 Feb 2011; revised 6 Mar 2011; accepted 9 Mar 2011; published 24 Mar 2011
(C) 2011 OSA

Let us view the local energy accumulation as a fluid 'queuing' system, as sketched in Fig. 9, in which periodic incoming energy packets of random sizes are accumulated and then dissipated inside the bulk. We identify mainly two dissipation mechanisms that will coexist i) a time-continuous systematic energy release due to heat dissipation which in itself cannot be responsible for the patterns generation and ii) a succession of sudden energy releases associated with bubble nucleation. Let us, from now on, focus on the second dissipative process which is due to the auto-siphoning mechanism arising in the set-up shown in Fig. 9. From this qualitative picture, we extract the following features:

3.2.1. Regularization effects due cumulative process

The local energy storage realized via the accumulation of energy packets can be viewed as the sum of random variables drawn from a common probability stationary distribution. Our experimental conditions require a large number, (i.e. typically of the order of several times 10^4) of successive laser pulses for the local energy to exceed the threshold W_{cr}. This enables us to invoke the probabilistic law of large numbers implying that the variance of the sum of N individual independent energy contributions decreases with $\sqrt{N}$. For large N, the average number of pulses required to locally exceed W_{cr} becomes a quasi-deterministic quantity. This in turn implies that the time between successive energy releases to be quasi-deterministic, leading to the very regular, noise-independent, bubble patterns experimentally observed.

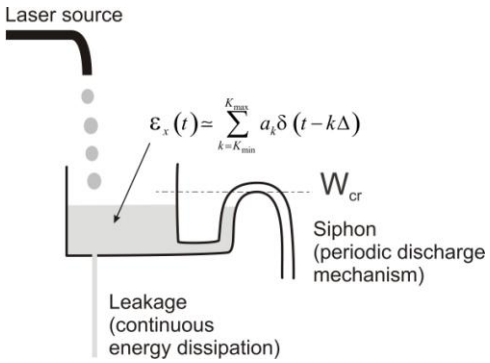

Fig. 9. Qualitative fluid analogy of the laser energy accumulation-discharge process. When the water level in the vessel fills the siphon elbow, (i.e high W_{cr}), auto-siphoning is triggered. For high elbows, (i.e. high W_{cr}), the auto-siphoning purge of the system is triggered. For high elbows, random stationary fluctuations in the faucet flow are smoothed out due to the law of large numbers.

3.2.2. Transition from periodic to chaotic patterns

While the mechanism sketched in Fig. 9 explains heuristically the generation of periodic structures, it cannot alone explain the more complex structures observed when the translation velocity v is decreased). For instance, more complex patterns consisting of two or three small bubbles preceding a larger one are observed in certain conditions (see Fig. 1). For the lowest velocities, chaotic bubble structures are clearly observed in the experiment. To include these phenomena into our modeling, the simple siphon model presented in Fig. 9 has to be refined.

This is achieved by introducing a single control parameter α and discrete time dynamic modeling (see Fig. 10):

$$\begin{cases} \tau_{n+1} = \tau_n + \Xi_\alpha(\varphi_n) + S_\alpha(\tau_n, \varphi_n) + D_\alpha(\tau_n, \varphi_n) \\ \varphi_{n+1} = \gamma\varphi_n + \Theta_\alpha\left[\Xi_\alpha(\varphi_n)\right] \end{cases} \quad (2)$$

#142538 - $15.00 USD Received 10 Feb 2011; revised 6 Mar 2011; accepted 9 Mar 2011; published 24 Mar 2011
(C) 2011 OSA

The first term describes the energy storage and the second one the residual energy balance. In these equations, τ_n is the time when the n^{th} energy discharge ends and φ_n is the local energy left after the n^{th} discharge.

Starting at a level φ_n at time τ_n, the function $\Xi_\alpha(\varphi_n)$ characterizes the time interval required to reach the threshold level W_{cr}. The function $S_\alpha(\tau_n,\varphi_n)$ describes the energy purging time interval from level W_{cr} to level φ_{n+1}. The function $D_\alpha(\tau_n,\varphi_n)$ stands for a delay resulting from the laser impacting a bubble region instead of the bulk.

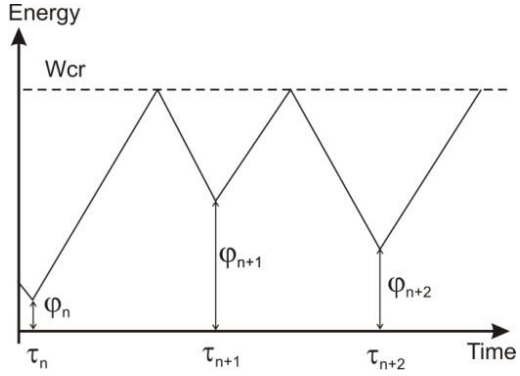

Fig. 10. Qualitative sketch of the iterative mapping (see Eq. (2)).

Indeed, the bubble formation velocity, due to an explosion shockwave, exceeds the laser translation velocity v and hence the laser beam will impact on bubble regions. The functions $\Xi_\alpha(\varphi_n)$, $S_\alpha(\tau_n,\varphi_n)$ and $D_\alpha(\tau_n,\varphi_n)$ are controlled by the single parameter α which is the effective energy input rate - α effectively lumps the joint effects of the energy laser pulse and the translation velocity v, in particular, the smaller v, the larger α becomes and for fixed laser pulse energy, the α will be only v-dependent. Finally, the function $\Theta_\alpha[\Xi_\alpha(\varphi_n)]$ introduces a nonlinearity into the local energy storage balance and we shall further detail its physical content below.

Adopting such a discrete time map, we observe that the dynamics of the simple siphon mechanism represented in Fig. 9 can be a discrete time mapping of the form:

$$\begin{pmatrix} \tau_{n+1} \\ \varphi_{n+1} \end{pmatrix} = \underbrace{\begin{pmatrix} 1 & \alpha \\ 0 & 1 \end{pmatrix}}_{:=M} \begin{pmatrix} \tau_n \\ \varphi_n \end{pmatrix} + \begin{pmatrix} S+D \\ 0 \end{pmatrix} \tag{3}$$

Which is derived from Eq. (2) provided that we choose:

$$\begin{aligned} &\Xi_\alpha(\varphi_n) = \alpha\varphi_n, \\ &\Theta_\alpha\left[\Xi_\alpha(\varphi_n)\right] = \left[(1-\gamma)/\alpha\right]\Xi_\alpha(\varphi_n), \\ &S_\alpha(\tau_n,\varphi_n) = S, \\ &D_\alpha(\tau_n,\varphi_n) = D. \end{aligned}$$

The stationary periodic auto-siphoning oscillations that solve Eq. (2) are given by:

$$\tau_n = \tau_0 + nP, \qquad \varphi_n \equiv \varphi_s = (P-S-D)/\alpha \tag{4}$$

where P is a constant defining the siphon period which can be calibrated from W_{cr}. Note that the mapping in Eq. (3) is conservative as the determinant of M is unity. This conservation

#142538 - $15.00 USD Received 10 Feb 2011; revised 6 Mar 2011; accepted 9 Mar 2011; published 24 Mar 2011
(C) 2011 OSA

character enables the sustained oscillations of the auto-siphoning mechanism (in accordance with the observations).

To further simplify, we assume that the time interval for the energy discharges is extremely short compared with other characteristic times, i.e. $S(\tau_n,\varphi_n) \approx 0$.

In addition, we assume the delay term to be approximately constant and equal to D. Finally, we rescale the time as $\tau_n = \alpha\, t_n$. With these assumptions, Eq. (3) becomes:

$$\begin{cases} t_{n+1} = t_n + \dfrac{1}{\alpha}\Xi_\alpha\left(\varphi_n\right) + \dfrac{D}{\alpha} \\ \varphi_{n+1} = \gamma\varphi_n + \Theta\left[\dfrac{1}{\alpha}\Xi_\alpha\left(\varphi_n\right)\right] \end{cases} \tag{5}$$

In this representation, the residual energy balance is idealized by two terms. The first is a linear dissipative part which for $\gamma \in [0,1]$ which implies that at time t_{n+1} the residual energy can only be a portion of its previous value at time t_n. The second is a nonlinear energy input $\Theta\left[\alpha^{-1}\Xi_\alpha\left(\varphi_n\right)\right]$ which accounts for an effective auto-regulating mechanisms which underlies the bubble nucleation process.

For consistency, the functional $\Theta\left[\alpha^{-1}\Xi_\alpha\left(\varphi_n\right)\right]$ has to be bounded so that:

$$\varphi_{n+1} = \gamma\varphi_n + \Theta\left[\frac{1}{\alpha}\Xi_\alpha\left(\varphi_n\right)\right] > 0 \qquad \forall t_n .$$

The existence of sustained oscillations which do correspond to solutions of Eq. (5) of the form $\varphi_n = \varphi_s$ and $t_n = t_0 + nP$, $\forall n$ implies in Eq. (5) the existence of a conservation mechanism of the form:

$$\Theta\left[P + \frac{1}{\alpha}\Xi_\alpha\left(\varphi_n\right)\right] = \Theta\left[\frac{1}{\alpha}\Xi_\alpha\left(\varphi_n\right)\right]$$

Based on experimental observations, we further assume an approximately linear energy accumulation leading to W_{cr} which, in the rescaled time, implies $\alpha^{-1}\Xi_\alpha\left(\varphi_n\right) = \varphi_n + \varepsilon\left(t_n,\varphi_n\right)$.

The small nonlinear correction $\varepsilon(t_n,\varphi_n)$, to be from now on neglected, could account for transient oscillatory effects underlying the bubble nucleation. Finally, the simplified model is written:

$$\begin{cases} t_{n+1} = t_n + \varphi_n + \dfrac{D}{\alpha} \\ \varphi_{n+1} = \gamma\varphi_n + \Theta_\alpha\left(t_{n+1}\right) \end{cases} \tag{6}$$

A direct substitution shows that the mapping Eq. (6) admits simple periodic solutions of the form:

$$t_n = t_0 + kP, \quad k \in \mathbb{N} \quad and \quad \varphi_n = \varphi_s, \quad \forall n \in \mathbb{N} \tag{7}$$

with $t_0 \in [0,1]$ and P two constants. While P calibrates the modeling, the stationary phase t_0 is determined by:

$$\Theta\left(t_0 + \varphi_s\right) + \left(\gamma - 1\right)\varphi_s = 0 \tag{8}$$

A linear stability analysis of the simple periodic solution given by Eq. (8) as a function of the control parameter α can now be worked out. The resultant linear mapping $L_\alpha(t_0,\varphi_s)$ reads as:

#142538 - $15.00 USD Received 10 Feb 2011; revised 6 Mar 2011; accepted 9 Mar 2011; published 24 Mar 2011
(C) 2011 OSA

$$L_\alpha(t_0,\varphi_s)=\begin{pmatrix}1 & 1\\ \dfrac{\partial\Theta_\alpha}{\partial t} & \gamma+\dfrac{\partial\Theta_\alpha}{\partial\varphi}\end{pmatrix}_{(\varphi=\varphi_s,t=t_0)}=\begin{pmatrix}1 & 1\\ \Theta'_\alpha & \gamma+\Theta'_\alpha\end{pmatrix} \quad (9)$$

and the stability of the periodic solution (t_0,φ_s) will be ensured provided the spectrum of $L_\alpha(t_0,\varphi_s)$ is confined inside the unit circle [23], namely:

$$\left|\lambda_\pm\right|=\left|\frac{1}{2}\left\{\left[1+\gamma+\Theta'_\alpha\right]\pm\sqrt{\left[1+\gamma+\Theta'_\alpha\right]^2-4\gamma}\right\}\right|<1 \quad (10)$$

or equivalently:

$$\left|\lambda_+ +\lambda_-\right|=\left|\left[1+\gamma+\Theta'_\alpha\right]\right|<2 \quad and \quad \lambda_+.\lambda_-=\gamma. \quad (11)$$

The explicit α-dependency of Θ'_α may alter the stability condition $\left|\left[1+\gamma+\Theta'_\alpha\right]\right|<2$, leading to a bifurcation of the dynamics to a new periodic solution. This is precisely encountered in the dynamics obtained from Eq. (8) when $\Theta_\alpha(t_{n+1})=-\alpha\cos(t_{n+1})$ [23]. This kind of dynamics, commonly referred to as bouncing-ball dynamics, exhibits a Feigenbaum cascade of period doubling bifurcations ultimately ending in the chaotic regime [23,24]. We do believe that, despite its truly synthesized character, our modeling approach captures the basic features leading to the complex patterns generation observed in the experiment. To demonstrate our point, in the next paragraph, we describe experimental observations featuring a Feigenbaum cascade type of behavior.

3.2.3. Experimental observations of period doubling phenomena and chaos formation

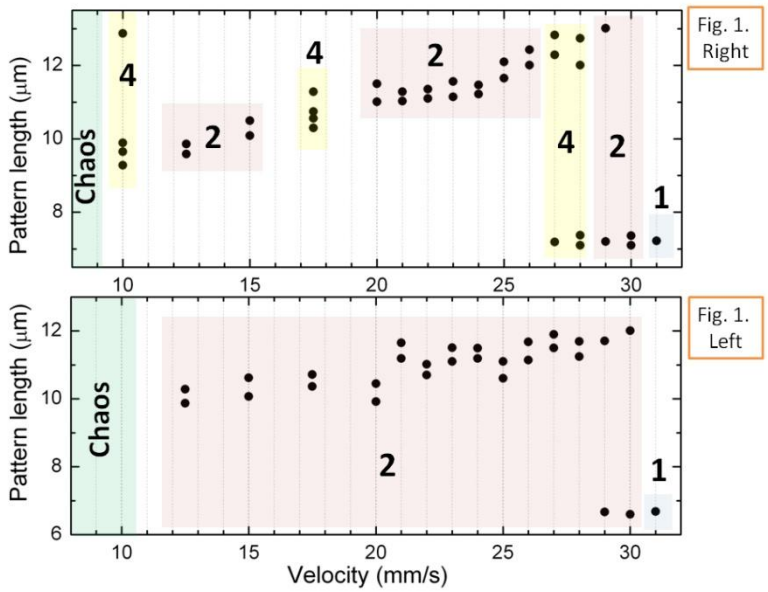

Fig. 11. Pattern length distributions as a function of the laser writing velocity for the two sets of experiments presented in Fig. 1. We define the pattern length as the length measured along the writing direction of the bubble patterns (see Fig. 7). Each point corresponds to the average of measured pattern length separated by less than three times the standard deviation of the measurement methods. The various regimes are highlighted and the figure illustrates a series of cascade of bifurcations as theoretically predicted.

#142538 - $15.00 USD Received 10 Feb 2011; revised 6 Mar 2011; accepted 9 Mar 2011; published 24 Mar 2011
(C) 2011 OSA

It is fair to assume that the energy effectively released in the system is intimately correlated, although not necessarily one-to-one, to the length of the bubble patterns (as measured along the laser-writing direction). To better assess the existence of a cascade of bifurcations, the pattern length distributions are measured for the two experiments presented in Fig. 1. The results are shown in Fig. 11. In this graph, each point corresponds to the average of measured pattern lengths that are distant one from another by less than three times the estimated standard deviation of the measurement method. The estimated standard deviation is calculated from the patterns length obtained at the highest writing speed (>30 mm/s) where single and highly regular bubbles are found for both writing direction described in Fig. 1.

The results in Fig. 11 explicitly unveil the existence of a cascade of period doubling regimes, from single to double or even quadruple - in the case of Fig. 1, right. This succession of dynamic regimes of the Feigenbaum type observed at the bubbles level, is the direct signature of the actual underlying dissipation mechanism. Tuned by the reduction of the laser translation velocity, the initial simple periodic dissipation pattern ends to chaos via a bifurcating cascade of dissipation mechanisms with increasing complexity. The observed bubble patterns form a reliable signature of the nonlinear dissipative mechanism. Note that for dripping faucets and bubbles generators in liquids, a similar modeling approach has also been adopted in the recent contributions of [25].

4. Conclusion

We have demonstrated the formation of self-organized periodic patterns consisting of single or multiple bubbles assembly in fused silica. These patterns were obtained by continuously scanning a low-energy laser beam emitting femtosecond laser pulses. Our data collected in the cumulative regime show a transition from a chaotic to a periodic regime as the laser writing speed is increased. In particular, we report the formation of alternating regular patterns of varying complexities, eventually converging to a single bubble pattern at the highest writing speed.

Our study emphasizes the complexity of the phenomena involved in the formation process of these patterns. In particular, we note the occurrence of bubble nucleation, bubble coalescence as well as possible hydro-thermodynamics events.

Despite the intrinsic complexity of the phenomena, we show that the transition from a chaotic to a periodic regime can be captured by a stylized model involving only a few variables. Our experimental observations confirm the existence of a cascade of bifurcations such described by Feigenbaum and validate qualitatively our modeling approach.

Finally, we demonstrated the high-speed writing (>30 mm/s) of two- and three-dimensional bubble networks in the bulk of fused silica.

Acknowledgments

This work is supported by the European Commission through the Seventh Framework program. Femtoprint (www.femtoprint.eu), NMP, project no 260103. Yves Bellouard thanks the Institute of Microengineering (IMT) of EPFL for the invited professorship during which this paper was finalized.

#142538 - $15.00 USD Received 10 Feb 2011; revised 6 Mar 2011; accepted 9 Mar 2011; published 24 Mar 2011
(C) 2011 OSA